Journal of Power Sources 216 (2012) 227–236

Contents lists available at SciVerse ScienceDirect

Journal of Power Sources

journal homepage: www.elsevier.com/locate/jpowsour

Development and characterization of glass-ceramic sealants in the ($CaO–Al_2O_3–SiO_2–B_2O_3$) system for Solid Oxide Electrolyzer Cells

Hichem Khedim [a], Hélène Nonnet [a,*], François O. Méar [b,c]

[a] CEA, DEN, DTCD, SECM, LDMC, Marcoule, F-30207 Bagnols-sur-Cèze, France
[b] Université Lille Nord de France F-59000 Lille, France
[c] Unité de Catalyse et de Chimie du Solide, UMR-CNRS 8181, USTL F-59652, France

HIGHLIGHTS

- New glass-ceramic formulation for sealing applications.
- Influence of heat treatment on the seal behavior and crystallization process.
- Glass-ceramic/Metal and glass-ceramic/ceramic interfaces and interactions.
- Effect of V_2O_5, K_2O and TiO_2 on thermal properties.
- Determination of crystallization kinetic parameters of the selected composition.

ARTICLE INFO

Article history:
Received 23 February 2012
Received in revised form
11 May 2012
Accepted 16 May 2012
Available online 23 May 2012

Keywords:
Solid Oxide Electrolyzer Cell (SOEC)
Sealing materials
Glass-ceramic
Metal–glass interface

ABSTRACT

The efficiency of glass-ceramic sealants plays a crucial role in Solid Oxide Electrolyzer Cell performance and durability. In order to develop suitable sealants, operating around 800 °C, two parent glass compositions, CAS1B and CAS2B, from the $CaO–Al_2O_3–SiO_2–B_2O_3$ system were prepared and explored. The thermal and physicochemical properties of the glass ceramics and their crystallization behavior were investigated by HSM, DTA and XRD analyses. The microstructure and chemical compositions of the crystalline phases were investigated by microprobe analysis. Bonding characteristic as well as chemical interactions of the parent glass with yttria-stabilized zirconia (YSZ) electrolyte and ferritic steel-based interconnect (Crofer®) were also investigated. The preliminary results revealed the superiority of CAS2B glass for sealing application in SOECs. The effect of minor additions of V_2O_5, K_2O and TiO_2 on the thermal properties was also studied and again demonstrated the advantages of the CAS2B glass composition. Examining the influence of heat treatment on the seal behavior showed that the choice of the heating rate is a compromise between delaying the crystallization process and delaying the viscosity drop. The thermal Expansion Coefficients (TEC) obtained for the selected glass ceramic are within the desired range after the heat treatment of crystallization. The crystallization kinetic parameters of the selected glass composition were also determined under non-isothermal conditions by means of differential thermal analysis (DTA) and using the formal theory of transformations for heterogeneous nucleation.

1. Introduction

Continuous economic and demographic growth along with higher living standards leads to a rising demand for energy. On the other hand, the depletion of fossil fuel reserves and the emission of greenhouse gases constitute a menace to the present and the future generations in terms of energy availability, environmental pollution, global warming and health hazards. Hydrogen has been identified as a potential alternative fuel as well as an energy carrier for the future energy supply. Water electrolytic hydrogen is currently the most practical and promising technology and especially the most environmentally friendly manner for large-scale renewable hydrogen production.

Research into hydrogen production using high temperature electrolysis methods have increased significantly in the last few years [1]. High Temperature Electrolysis (HTE) using Solid Oxide Electrolyzer Cells (SOECs) is a promising method involving electrochemical reactions that convert electric power into chemical energy. Although the SOEC technology has indeed been developed,

* Corresponding author. Tel.: +33 4 66 79 16 75; fax: +33 4 66 79 18 80.
E-mail address: helene.nonnet@cea.fr (H. Nonnet).

0378-7753/$ – see front matter © 2012 Elsevier B.V. All rights reserved.
doi:10.1016/j.jpowsour.2012.05.041

manufacturing of SOEC stacks requires the development of gas-tight seals, as rapid degradation of the cell performance is observed when small leaks are present [2]. Sealing is required along the edges of the electrodes, electrolyte and interconnect, as well as between individual cell stacks, to prevent mixing of gases in the anode and the cathode, and to provide electrical insulation to prevent shunting. The production of reliable joints is currently the main limitation in the production units and justifies the research effort in this field [3–5]. The requirements for the sealants are stringent as they need to withstand severe environmental conditions at high operating temperature (800 °C) in SOEC stacks. The sealants must simultaneously meet several requirements such as gas tightness, chemical inertness to the adjoining cell components, electrically insulation, and coefficient of thermal expansion (CTE) compatibility with other cell components, suitable viscosity, and good adherence with the adjoining components [3,4,6,7].

Sealing materials can be classified in two categories: (i) Compressive seals such as metallic or mica-based, and (ii) rigid seals such as glass, glass-ceramics, or brazes [4,8]. Many studies were dedicated to the formulation and characterization of these sealing matrix [4,7,9–12]. However, glass and glass-ceramics with carefully tailored chemical compositions are able to meet most of the requirements [13–15]. Glass and glass-ceramic sealants exhibit strong bonding to the interface; their adherence to the cell provides hermetic sealing. Although glass present the faculty of self-healing, which can be very beneficial in case of cracking [16–20], their excessive devitrification at operating temperatures leads to drastic changes in their physicochemical properties. This shortcoming can be avoided by employing glass-ceramics sealants whose crystallization can be controlled. However, for such materials the self-healing faculty is partially or even completely lost; therefore, glass-ceramic properties have to be completely determined, starting from their vitreous state, in order to be perfectly adapted to adjacent cell components. Their performance depends on their components, compositions and arrangement in the network structure which is very complex and not yet fully understood. The formulation process of a glass ceramic is highly complex especially due to the large number of elements that can be included.

Glass-ceramics from several systems have been investigated and their suitability for sealing applications within SOECs have been discussed in previous work [21,22]. It was concluded that glass-ceramics based on the $CaO–Al_2O_3–SiO_2$ (CAS) system meet most of the requirements for efficient sealing, especially in terms of chemical durability. The objective of this work is to determine the most suitable CAS-based glass-ceramic composition for sealing applications. Given the refractory character of the CAS-based glass and their high viscosity at the SOEC operating temperatures (<900 °C), two parent glass compositions (CAS1 & CAS2) were selected on the basis of their liquidus temperatures (T_L) which correspond to the lowest melting points in the CAS system, 1170 and 1265 °C respectively for CAS1 and CAS2 (Fig. 1 & Table 1). About 6 wt% of B_2O_3 was systematically added to the parent glass compositions as a flux. CAS1 and CAS2 glass compositions containing 6 wt% B_2O_3 are designated CAS1B and CAS2B.

A comparative study of both glass compositions, based on experimental data, was carried out and one of the compositions was selected. Optimized compositions have been defined with minor additions of V_2O_5, K_2O and TiO_2. The crystallization kinetics of the optimized glass composition were investigated by Differential Thermal Analysis (DTA).

2. Experimental procedure

2.1. Glass preparation

Batches were prepared from reagent grade SiO_2, Al_2O_3, $CaCO_3$, H_3BO_3, V_2O_5 and KNO_3. The thoroughly mixed batches were placed in a Pt/10% Rh crucible and heated to 900 °C in a muffle furnace for 1 h in order to eliminate carbonates and nitrates, after which the batches were melted at 1550 °C for 3 h. The melt was then poured

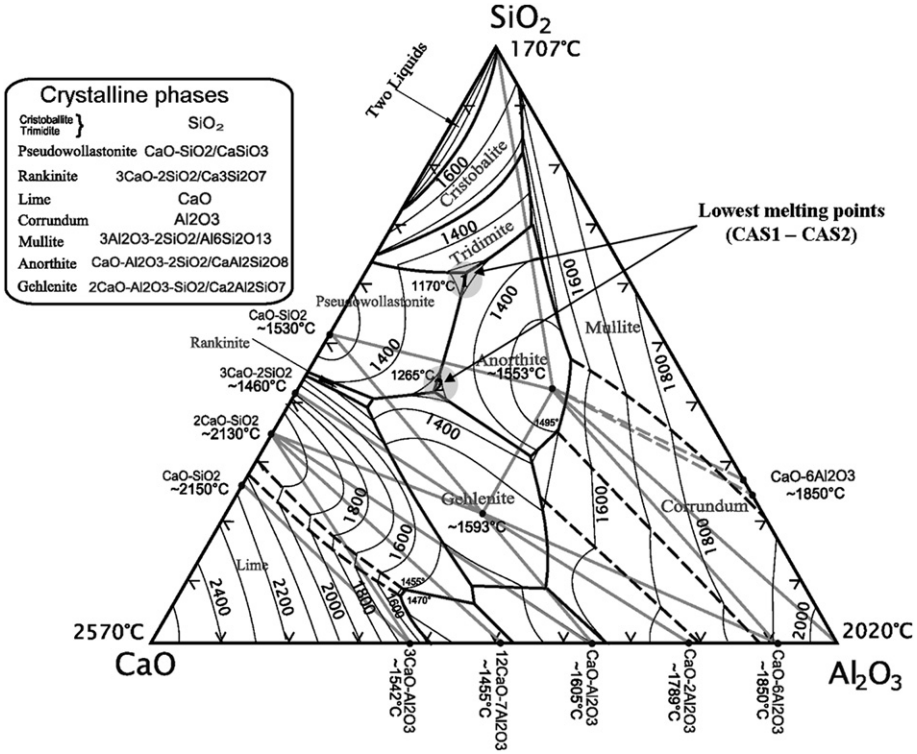

Fig. 1. CAS1 and CAS2 glass positions on the $CaO–Al_2O_3–SiO_2$ pseudo ternary phase diagram (wt%).

Table 1
Chemical compositions of glass used in this work (wt%).

Name	CaO	Al_2O_3	SiO_2	B_2O_3	TiO_2	V_2O_5	K_2O
CAS1	24.5	14.0	61.5	–	–	–	–
CAS2	37.5	20.3	42.2	–	–		
CAS1B	22.83 (0.38)	12.76 (0.12)	58.36 (0.34)	6.25 (0.42)	–	–	–
CAS2B	35.80 (0.17)	18.24 (0.11)	39.30 (0.47)	6.03 (0.13)	–	–	–
CAS2BT	34.74 (0.55)	5.81 (0.29)	38.13 (0.82)	5.81 (0.29)	2.36 (0.2)	–	–
CAS2B2V	34.54 (0.23)	17.74 (0.15)	39.18 (0.21)	6.13 (0.15)	–	2.14 (0.05)	–
CAS2BK	35.52 (0.15)	16.90 (0.09)	37.82 (0.11)	5.34 (0.19)	–	–	4.57 (0.05)

Values in parentheses are the standard deviations.

onto a metal plate and crushed. The latter step was repeated twice in order to homogenize the bulk. Part of the poured sample was crushed and milled in a laboratory mixer mill for 1 h and then sieved to a particle size below 20 μm.

The parent glass and their derivatives obtained at the glass manufacturing step were transparent and free from any crystalline phases. Glass compositions were systematically checked by electron probe microanalysis, and are indicated in Table 1.

2.2. Sample preparation

For glass/substrate interaction tests, the glass powder was blended with an organic binder, based on polyvinyl butane, in order to form a viscous glass paste. The thick paste was then applied with a dispensing syringe in a sandwich conformation between Crofer® and YSZ surfaces. The sealing heat treatment was then performed on the samples in an electric furnace.

The development of crystalline phases was investigated by isothermal heat treatment of powder samples in an electric furnace in air. The samples were heat treated for 2–50 h at 850 °C.

2.3. Heat treatment

The choice of the appropriate heat treatment depends on the thermal properties of the glass. In theory, a typical treatment involves initially spreading of the glass over the substrate followed by crystallization of the glass. In reality, these two steps would be in competition since crystallization can occur as the glass spreads. The sooner crystallization occurs; the sooner the glass viscosity will drastically increase, possibly blocking the natural viscous flow of the glass. Therefore, the crystallization mechanism of the sealing glass ceramic should be controlled and taken into account when establishing the heat treatment. For this reason, no nucleation step was used during heat treatment. In order to avoid damaging the SOEC components, the heating rate never exceeded 3 °C min^{-1}.

The heat treatment recommended for this study was based on the following sequences as schematized on Fig. 2:

- Step (a): $T \approx 400$ °C; $t = 1$ h, for debinding of the glass paste;
- Step (b): $T_S < T < 900$ °C; $t \approx 15$ min, for softening and seal bonding to the joined materials;
- Step (c): $T = 850$ °C; 24 h $< t <$ 50 h, for crystallization of the glass;
- Step (d): $T = 800$ °C; $t = 100$ h, for homogenization at the SOEC operating temperature.

2.4. Physicochemical characterization

Thermal properties of the synthesized glass, such as glass transition temperature (T_G), softening temperature (T_S) and temperature of maximum crystallization (T_x), were measured by differential thermal analysis using a TG-DTA92 (Setaram) with a heating rate of 10 °C min^{-1} from room temperature to 1200 °C in argon atmosphere. The crystallization kinetics were studied by an isothermal investigations using DTA scans recorded from room temperature to 1200 °C in flowing dry argon at various heating rates from 1 to 30 °C min^{-1}. The development of crystalline phases in the glass after isothermal heat treatments at 850 °C for different durations was identified from powder X-ray diffraction (XRD) patterns recorded at room temperature using a Bragg Brentano diffractometer in $\theta/2\theta$ geometry, with a Cu anticathode.

Microstructures of polished cross sections of heat treated specimens (glass + substrate) were observed using a Philips XL30 scanning electron microscope (SEM). Quantitative chemical analysis was performed on unheated and heat-treated glass using a CAMECA SX 100 Electron Probe Microanalyzer (EPMA) equipped with five wavelength-dispersive spectrometers (WDS). The elements analyzed were Ca, Al, Si, B, V, Ti and K. The concentration of oxygen was calculated by stoichiometry assuming that the valences of the cations are respectively 2, 3, 4, 3, 5, 4 and 1.

The sintering behavior of the glass powders was investigated using a Hot-Stage Microscope (HSM). The computerized image analysis system automatically records and analyzes the sample geometry changes during heating. The measurements were conducted in air; the heating rate from room temperature to 500 °C was 50 °C min^{-1} because in this range the heat treatment does not affect the glass behavior. Above 500 °C, the heating rate was maintained at 3 °C min^{-1} until flow behavior was observed. Cylindrical samples prepared by cold-pressing the glass powder were placed on a Crofer® substrate. Photos were taken at different stages of the process showing the change in shape of the silhouetted sample. The variation in the area and height of the silhouette was defined as A/A_0 (where A is the surface area of the sample at T and A_0 is the initial surface area of the sample). This methodology,

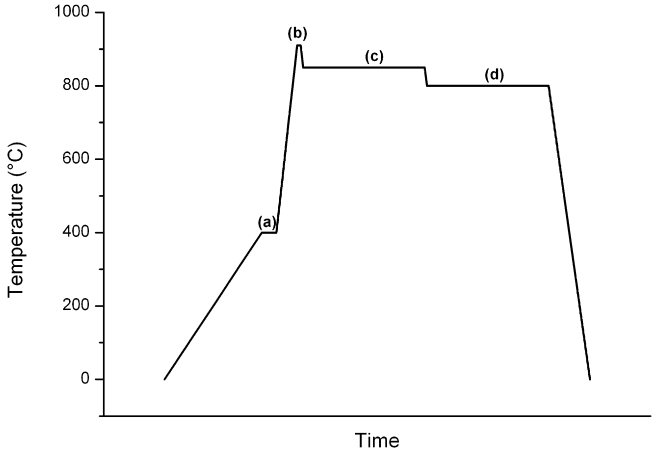

Fig. 2. Heat treatment schedule for this work.

Table 2
Summary of thermal and sintering parameters of glass obtained.

T(°C)	T_G[c]	T_S[c]	T_X[c]	T_{FS}[d]	T_{MS}[d]	T_C[d]	T_D[e]	T_{HB}[e]	T_F[e]
CAS1B	729	760	–	754	–	1005	932	978	1161
CAS2B	734	757	1018	752	838	909	873	–	1210
CAS2BT	730	757	1028	759	839	911	864	1190	1200
CAS2B2V	705	745	1002	740	811	853	852	–	1142
CAS2BK	712	751	1048	748	830	932	895	1175	1177
CAS2B[a]				*737*	*827*	*879*	*851*	–	*1188*
CAS2B[b]				*752*	*852*	*948*	*885*	*948*	*1232*

[a] Heating rate 1 °C min^{-1}.
[b] Heating rate 10 °C min^{-1} (recorded by HSM).
[c] Parameters extracted from DTA measurements at 10 °C min^{-1}.
[d] Parameters extracted from ($A/A_0 = f(T)$) curves plotted from HSM measurements at 3 °C min^{-1}.
[e] HSM photographs obtained from HSM imaging system.

based on the shadow method, allows the evolution of the sample shapes to be followed through the detection of glass deformations related to viscosity points. This provides a rapid assessment of the sealant flow and deformation characteristics over a broad temperature range.

3. Results and discussion

3.1. Thermal properties of investigated glass

Glass-ceramic formation involves the softening of glass powders followed by crystallization. The two processes have opposing effects on glass densification. In order to obtain good sealing, the softening stage must precede crystallization because dense and low porosity materials are desirable for obtaining a gas-tight glass-ceramic seal. When the crystallization rate is too high, the softening and the viscous flow of the glass are inhibited, leading to poor coating of the substrate by the glass.

Thermal properties (T_G, T_S and T_x) extracted from DTA measurements can provide qualitative information about glass behavior i.e. the glass transition temperature, the softening temperature, and the temperature corresponding to the maximum crystallization rate. Nevertheless, an accurate description of the glass behavior cannot be based only on DTA values. Pascual et al. [23] defined a new method for determining fixed viscosity points of glass based on HSM measurements. This new method leads to a correlation between the specific temperatures measured by HSM and their corresponding viscosities [23,24]. The HSM specific temperatures are:

- *First shrinkage or sintering* (T_{FS}): temperature at which the linear shrinkage of the glass starts (log $\eta = 9.1 \pm 0.1$). This step begins above T_G.
- *Point of maximum shrinkage* (T_{MS}): temperature of maximum shrinkage before the glass starts to soften (log $\eta = 7.8 \pm 0.1$)
- *Crystallization temperature* (T_C): temperature at which the crystallization rate is high enough to inhibit the softening process.
- *Softening/Deformation point* (T_D): temperature at which the first signs of softening are observed, highlighted by the disappearance of the small protrusions at the edges of the sample (log $\eta = 6.3 \pm 0.1$).
- *Half ball point* (T_{HB}): temperature at which the section of the sample observed forms a semicircle on the microscope grid (log $\eta = 4.1 \pm 0.1$).
- *Flow point* (T_F): temperature at which the height of the drop silhouette corresponds to a unit on the screen scale (log $\eta = 3.4 \pm 0.1$).

The thermal parameters based on DTA and HSM measurements are indicated in Table 2. This section describes the temperature dependence of glass behavior, compares the CAS1 and CAS2 parent glass, and describes the effect of each additive element based on HSM and DTA results.

It is generally believed that sealing can be effective when the sample reaches a half-ball shape. The investigated glass are intended for sealing applications within SOECs where the heat treatment cannot exceed $T_{Max} = 900$ °C; it is thus very important to determine their morphologies at this temperature.

3.1.1. Comparison between CASB1 and CAS2B

The crystallographic, chemical and thermal characterizations of the CAS1B and CAS2B glass will be used as a point of comparison between CAS1 and CAS2 parent glass. XRD analyses of the CAS1B and CAS2B glass powders heat treated at 850 °C for different durations (4, 25 and 64 h) reveal the crystallization behavior along with several phases (Figs. 3 and 4). It can be shown that crystallization is more rapid in the case of CAS2B glass since all the phases are already formed in the first 4 h whereas CAS1B glass is mainly amorphous for the same heat duration. The long term heat treatment pattern (64 h) shows that the main crystalline phases created in the CAS1B glass composition are SiO_2 (S), $CaAl_2Si_2O_8$ (CA_2S_2) and $CaSiO_3$ (CS); the crystalline phases in the case of CAS2B glass are $Ca_2Al_2SiO_7$ (C_2A_2S), $CaAl_2Si_2O_8$ (CA_2S_2) and $CaSiO_3$ (CS). The crystalline phases identified in both glass compositions are consistent with those expected from the phase equilibrium diagram (Fig. 1).

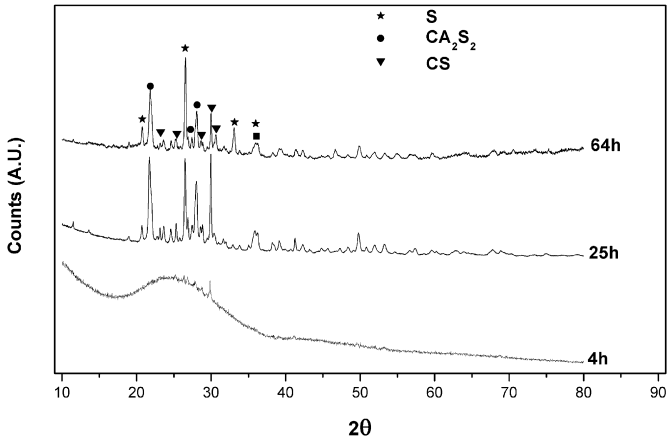

Fig. 3. XRD pattern of CAS1B glass for different durations at 850 °C.

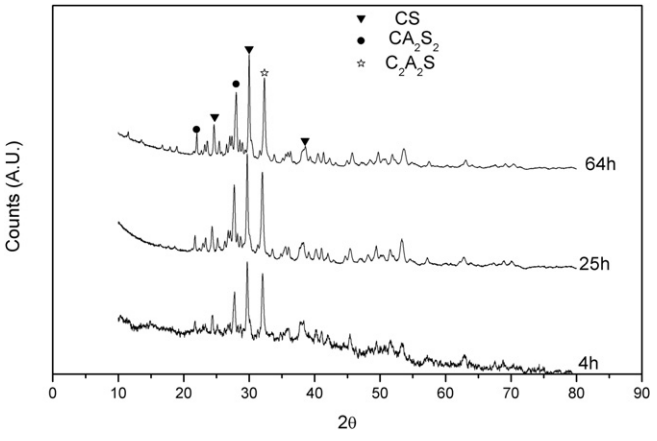

Fig. 4. XRD pattern of CAS2B glass for different durations at 850 °C.

Figs. 5 and 6 show the micrographs obtained for cross sections of CAS1B and CAS2B samples after long-term interaction tests ($T = 850$ °C, $t = 100$ h). The morphology of the crystalline phases identified from XRD patterns are presented in Figs. 5a and 6a.

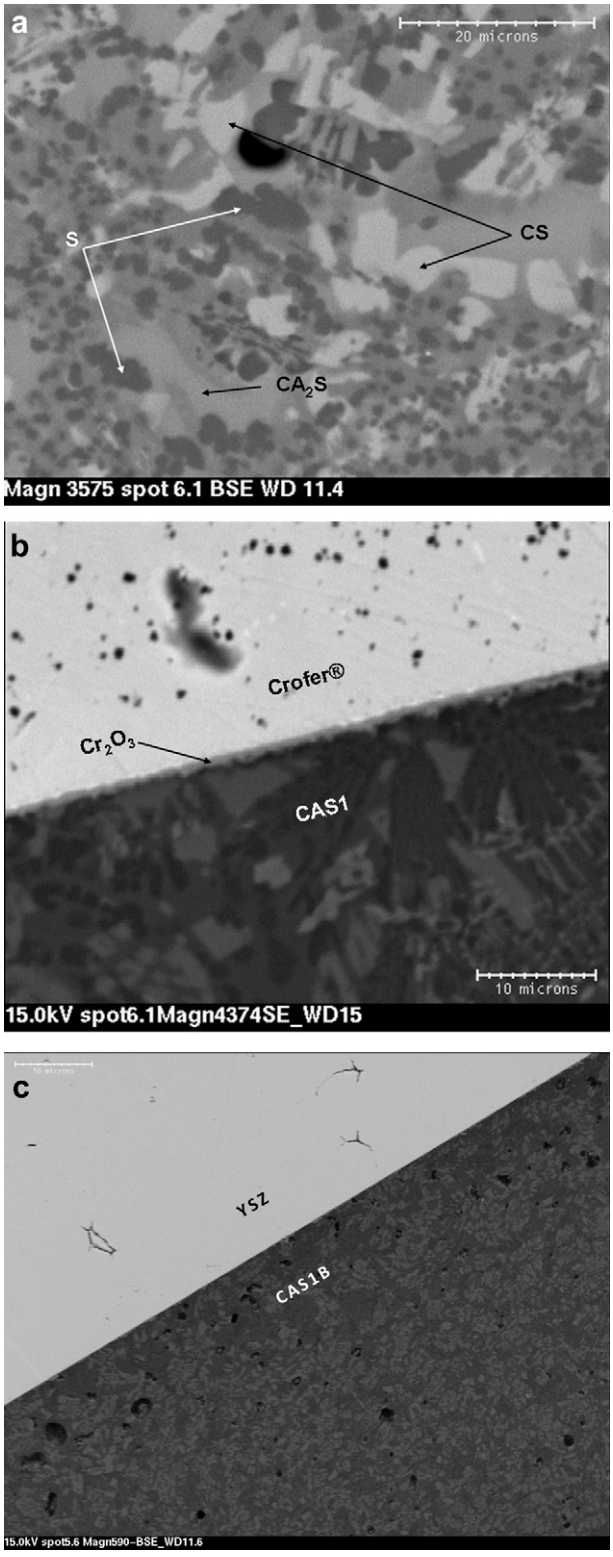

Fig. 5. Cross section of heat treated CAS1B sample (a) bulk glass (S = SiO_2; CA_2S_2 = $CaAl_2Si_2O_8$; CS = $CaSiO_3$); (b) metal/CAS1B interface; (c) ceramic/CAS1B interface.

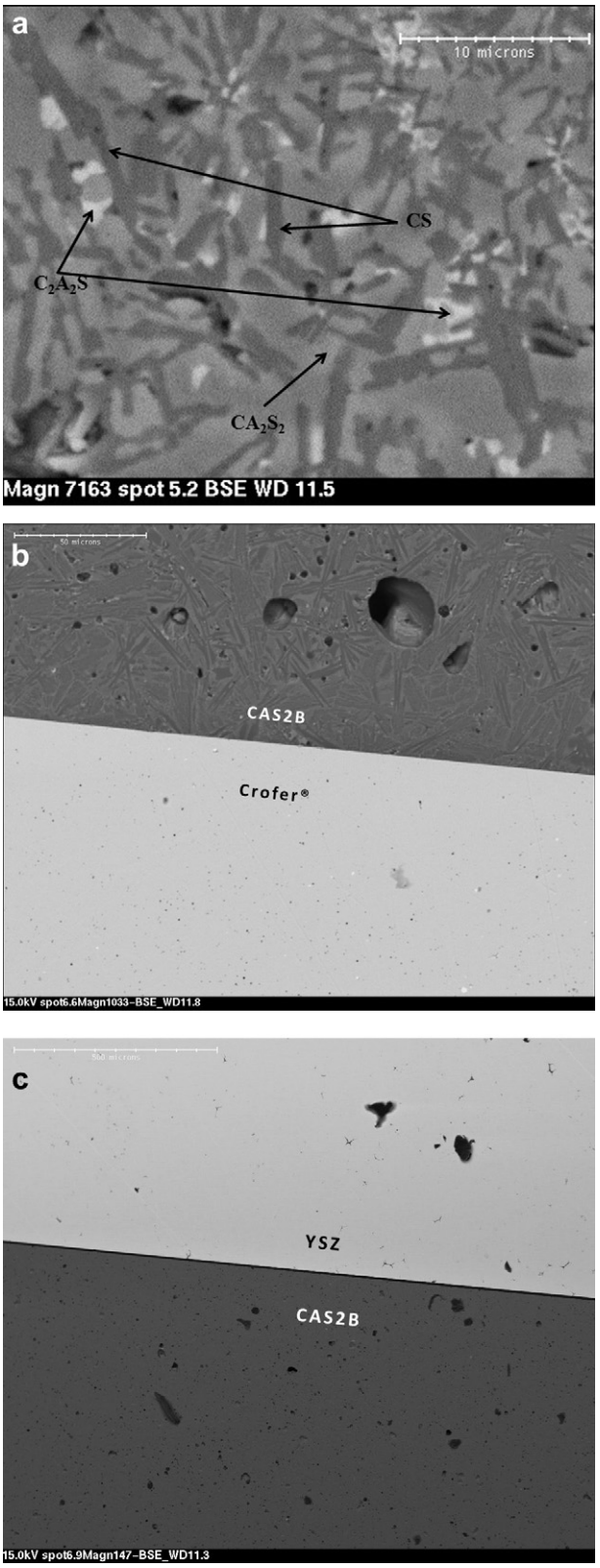

Fig. 6. Cross section of heat treated CAS2B sample (a) bulk glass (C_2A_2S = $Ca_2Al_2SiO_7$, SiO_2; CA_2S_2 = $CaAl_2Si_2O_8$; CS = $CaSiO_3$); (b) metal/CAS2B interface; (c) ceramic/CAS2B interface.

At the metal/glass-ceramic and ceramic/glass-ceramic interfaces, both glass show satisfactory interface quality (bonding, wetting and adherence behavior) that can satisfy the sealing requirement. However, an important difference between CAS1B and CAS2B interactions with metallic substrates is observed. At the interface between the glass sealant and the Crofer® alloy, a thin continuous and protective chromium-rich oxide layer was observed for CAS1B but not for CAS2B glass. SEM and EPMA chemical analyses performed on the residual amorphous phase near the metallic interface reveal that Cr is detected in both glass compositions. The chromium-rich oxide passivation layer formed at the metal/glass interface seems to be partially dissolved in the CAS1B glass composition and completely dissolved when in contact with CAS2B glass composition. This particular behavior can be explained by the difference in alkalinity between the two glass compositions. Recent studies have shown that under oxidizing conditions chromium oxide solubility increases with the melt alkalinity for a given temperature [25,26]. The glass alkalinity depends essentially on the alkali and alkaline earth oxide content, and significantly increases with increasing CaO/SiO_2 ratio. The CaO content in CAS2B is much higher than in CAS1B (Table 1). One way to maintain the chromia layer at the metal/glass interface is to supersaturate the parent glass composition with chromium oxide (<1 wt%).

Thermal properties of CAS1B and CAS2B glass obtained from DTA investigations (Table 2) show that the crystallization temperature peak was undetectable for CAS1B glass. Heat transfer induced by the crystallization mechanism in CAS1B glass seems to be below the detection threshold of the DTA analyzer. The glass transition and softening temperatures (T_G and T_S) are roughly the same for both glass, suggesting comparable temperature dependence of the glass.

The sample surface area variations (A/A_0) obtained from HSM investigations and plotted as a function of temperature for samples CAS1B and CAS2B (Fig. 7) show that the linear shrinkage process starts at about the same temperature (750 °C) for both glass (Table 2); this can be explained by the closeness of their T_G and T_S values. It can also be observed, in the case of CAS2B, that densification is continuous and maintained by the viscous flow of the sample before crystallization occurs at TC = 909 °C. For the CAS1B glass composition, the shrinkage and densification rates are much lower than for CAS2B glass. This behavior is due to a significant difference in viscosity between the two glass compositions. It is well known that increasing CaO content in silicate glass disrupts the silica network and consequently decreases the glass viscosity. The CaO content in the CAS2B glass is higher (Table 1) and thus

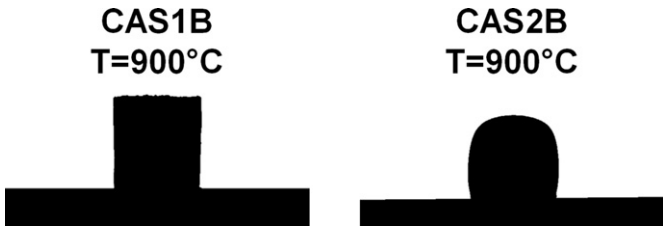

Fig. 8. HSM images of the sample CAS1B and CAS2B morphologies evolutions.

contributes to lowering the CAS2B glass viscosity compared with CAS1B. Nevertheless, a difference in viscosity of this magnitude cannot be attributed only to the effect of the difference in the CaO content between the two glass compositions. In addition, microprobe investigations performed on CAS1B glass reveal that the SiO_2 phase, which is one of the main crystalline phases in CAS1B glass, includes a large fraction of B2O3 as a solid solution (up to 10 wt%) dissolved from the glassy phase. The continuous formation of SiO2 during the crystallization process tends to deplete the remaining amorphous phase in B2O3 leading to a significant increase in glass viscosity which directly impacts the flow properties of the glass. This induces a densification/softening delay that prevents good spreading of the glass. The high viscosity of CAS1B glass consequently prevents reaching suitable glass morphology at 900 °C (Fig. 8a) compared with the practically half-ball shape of CAS2B glass (Fig. 8b). This disqualifies the CAS1B composition as sealant glass for use in SOECs. However, due to its low crystallization kinetics, CAS1B glass can be a good candidate for sealing applications if higher sealing temperatures are allowed ($T > 950$ °C) since the glass softening process is continuous until 1005 °C before crystallization blocks viscous flow of the glass.

In the remainder of this study only the CAS2B glass composition will be further investigated as a potential SOEC sealant.

3.1.2. Effect of additives

The HSM data for CAS2B glass including different additives (V_2O_5, K_2O and TiO_2) can be plotted to show the sample surface area variations versus the heating temperature (Fig. 9).

V_2O_5 was added to the parent glass composition CAS2B in order to enhance glass densification. Adding V_2O_5 decreases the shrinkage/softening parameters (T_G, T_{FS}, T_S and T_D) (Table 2). It appears that the addition of V_2O_5 decreases the glass viscosity since the characteristic temperatures measured by HSM are correlated with the viscosity points. This effect is interesting and suitable to

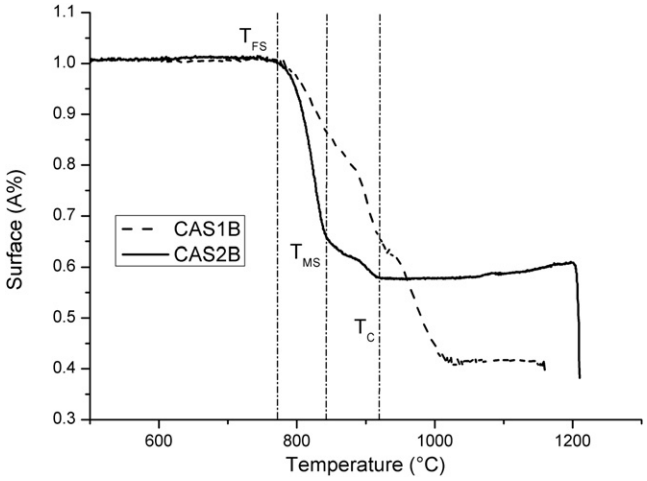

Fig. 7. Comparison between CAS1B and CAS2B HSM thermograms.

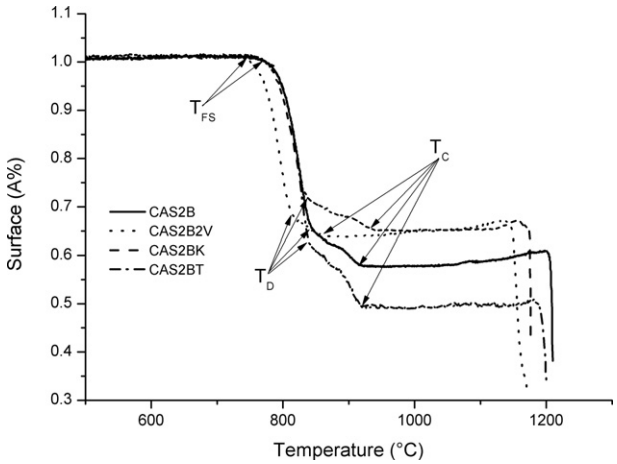

Fig. 9. Effect of additives (V_2O_5, K_2O and TiO_2) on glass sintering.

Fig. 10. HSM silhouettes of (CAS2)-based glass at maximum SOEC operating temperature (900 °C).

improve glass densification. On the other hand, V_2O_5 appears to be an effective nucleating agent since the peak crystallization temperature (T_x) and HSM crystallization temperature (T_C) also decrease (Table 2 and Fig. 9). As a consequence, crystallization prevents further densification of the glass, which is thus blocked at the beginning of the glass deformation process ($T_D \approx T_C$). A satisfactory glass morphology is therefore not reached at $T_{Max} = 900$ °C (Fig. 10c).

K_2O was added to the system as a flux in order to lower the glass melting point. The thermal parameters recorded for CAS2BK glass (Table 2) show that the presence of K_2O tends to decrease the T_G, T_{FS} and T_F values. It also can be observed that the crystallization temperatures T_C and T_x increase, which can be considered as useful behavior since the densification parameters are improved and crystallization is delayed. The deformation process, which occurs at the deformation temperature T_D, is associated with a viscosity of $\log \eta = 6.3 \pm 0.1$. This process occurs at $T_D = 895$ °C in the case of CAS2BK and at $T_D = 873$ °C for CAS2B. This indicates that the presence of K_2O, even if it acts as a fluxing agent, increases the viscosity of the glass. Consequently, the densification process is delayed and the half-ball shape would not be reached at $T_{Max} = 900$ °C (Fig. 10d).

TiO_2 was added to investigate the effect of a nucleating agent on glass behavior. DTA and HSM results show that adding TiO_2 affects neither densification nor crystallization: the thermal and densification parameters recorded for CAS2B and CAS2BT glass (Table 2) are very close. Moreover, the A/A_0 vs. temperature curves for both are practically superimposed. The only visible difference between the two curves is the value of the surface area ratio, A/A_0, at T_D and T_C. This difference is directly related to the sample preparation. The residual porosity and particle size distribution of the hand pressed samples are different and therefore so is the densification rate. However, for both compositions the sample silhouettes exhibit satisfactory densification and morphology at $T_{Max} = 900$ °C (Fig. 10a and d). It can thus be concluded that the addition of TiO_2, at least in the tested proportions (<2.4 wt%), has no effect on glass behavior.

At this stage, it can be concluded that the CAS2B glass composition meets the requirements for a sealing application and is selected for further investigations.

3.1.3. Effect of heating rate

The heating rate is imposed by SOEC manufacturers and generally must not exceed 5 °C min^{-1} in order to avoid thermal shocks between the stack components. Nevertheless, it is useful to know its effect on densification and crystallization processes in glass. We investigated this effect on CAS2BT glass by means of HSM measurements recorded at different heating rates (1, 3 and 10 °C min^{-1}). The results are indicated in (Table 2 and Fig. 11). On the one hand, increasing the heating rate increases the crystallization temperature (T_C) and consequently delays the crystallization process (Fig. 10). This behavior can be considered useful for sealing applications since a delay in crystallization provides more time for densification. On the other hand, the characteristic temperatures indicated in Table 2 show that the softening and deformation points (T_S and T_D) are shifted to higher temperatures when the heating rate is increased. As a result, the decrease in viscosity obtained by raising the temperature is delayed when the heating rate increases. This prevents satisfactory spreading of the glass, which must occur below $T_{Max} = 900$ °C.

The choice of an optimal heat treatment (heating rate) is a compromise between delayed crystallization and a delayed viscosity decrease. Both parameters must be taken into account because the glass morphology at a given temperature, especially at 900 °C, is determined by the evolution of these two parameters. This behavior is confirmed by the shapes of the glass samples recorded at 900 °C (Fig. 12). Although the optimum T_C value is given by the highest heating rate (10 °C min^{-1}) and the optimum viscosity by the lowest heating rate (1 °C min^{-1}), the best heating rate in this case is a 3 °C min^{-1} since it yields the most suitable glass sample morphology at $T_{Max} = 900$ °C.

3.2. Determination of TEC value for CAS2B glass

The HSM study of the thermal behavior of glass demonstrated that the CAS2B glass composition is best suited for sealing applications. The following examinations were therefore carried out on this composition. Thermal Expansion Coefficients (TEC) were determined for both untreated (glassy) and heat treated (glass-ceramic) samples. The TEC value of the untreated sample was measured on a glass rod, 1 cm in diameter and 1 cm long, obtained by cooling a glass melt in pre-heated carbon crucibles and then machining the resulting specimens. The TEC of the heat-treated sample was measured on a cylindrical pellet of similar dimensions obtained by uniaxial pressing of the CAS2B glass powder (<20 μm).

The results in Fig. 13 show that the TEC of the treated sample (glass-ceramic) (11×10^{-6} °C^{-1}) is in the desired range, i.e. between the TEC of the ceramic ($\approx 10.5 \times 10^{-6}$ °C^{-1}) and metal

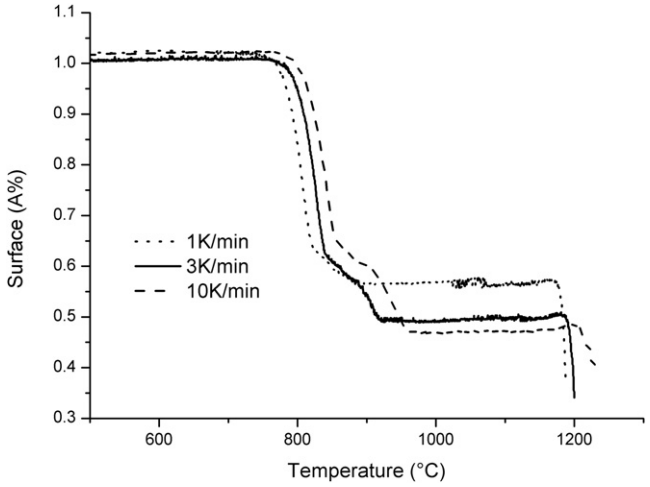

Fig. 11. Effect of heating rates on glass densification.

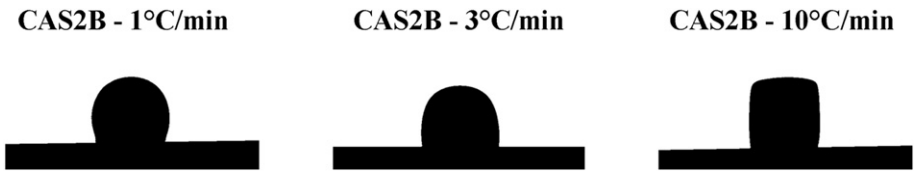

Fig. 12. CAS2B images at 900 °C for different heating rates.

($11.8 \times 10^{-6}\,°C^{-1}$) materials bonded to the glass-ceramic seal. These results confirm the suitability of the CAS2B glass composition for joining applications in SOEC.

3.3. Study of crystallization kinetics of CAS2B

The crystallization kinetics in the CAS2B glass composition were evaluated by means of DTA as described by Bansal et al. [27]. The Johnson–Mehl–Avrami (JMA) equation (eq. (1)) [28] describes the kinetics of phase transformation, such as crystallization of a glass, at a constant temperature:

$$-\ln(1-x) = (kt)^n \quad (1)$$

Where, x is the volume fraction of the glass crystallized after time t, n the dimensionless Avrami exponent which reflects the growth morphology (one-, two- or three-dimensional growth) and k the reaction rate constant. The temperature dependence of k (at least within narrow temperature ranges) follows an Arrhenius equation (eq. (2)):

$$k = \nu \exp\left(-\frac{E}{RT}\right) \quad (2)$$

Where E is the effective overall activation energy for the transformation process, υ an effective frequency factor which reflects the probability that a molecule having energy E participates in the transformation, R the gas constant and T the absolute reaction temperature.

During a non-isothermal DSC or DTA scan, the sample temperature changes linearly with time at a rate $\theta = dT/dt$ and then (eq. (3)),

$$T = T_i + \theta t \quad (3)$$

Where T_i is the initial temperature. In equation (eq. (1)) the right-hand side corresponds to the growth in volume of crystal nuclei. However, for non-isothermal heating, the reaction rate constant changes continuously with time due to the changing temperature, so that the JMA relation must be written as (eq. (4)):

$$-\ln(1-x) = \left(\int_0^t k(t)dt\right)^n \quad (4)$$

If at each temperature, the deflection of the DSC or DTA trace from its baseline is proportional to the instantaneous crystallization rate (Borchard assumption [29]), then the rate of sample transformation is maximum at the exothermic crystallization peak. Eq. (5) expresses T_x changes with the heating rate θ [30,31]:

$$\ln\left(\frac{T_X^2}{\theta}\right) = \ln\left(\frac{E}{R\nu}\right) + \frac{E}{RT_X} \quad (5)$$

Hence a plot of $\ln(T_X^2/\theta)$ versus $1/T_x$ should be linear with a slope of E/R and an intercept $\ln(E/R\nu)$. This equation is based on the assumption that at the maximum temperature in the crystallization exothermic peak, the crystallization rate reaches the same specific value independently of the heating rate. Earlier studies have shown that the crystallization kinetic parameters obtained by isothermal and non-isothermal DSC using this formalism are in good agreement, particularly when both studies are carried out in the same temperature range.

The crystallization onset (T_x) peaks recorded from DTA scans and obtained for the CAS2B glass at various heating rates (1–30 °C min^{-1}) are indicated in Table 3. Exothermic peaks of crystallization could not be detected for heating rates of 20 °C min^{-1} and higher.

T_x is seen to increase with the increasing heating rate (Table 3). This can be explained by the fact that at T_x, which corresponds to the maximum of the crystallization peak, observed in DTA scans, the rate of transformation of the viscous liquid into crystals reaches its maximum. When the crystalline phase has the same composition as the liquid, the transformation rate will depend on the density of crystallization sites. However, when the composition of the crystalline phase is different from that of the liquid, as in the present case, the rate of transformation will be controlled by the rate of diffusion through the viscous liquid and the number of crystallization sites to which diffusion can occur. If the number of nucleation sites is increased, e.g. by using lower heating rates, the maximum of the peak will occur at a temperature at which the melt viscosity is higher, i.e. at a lower temperature.

A plot of $\ln(T_X^2/\theta)$ versus $1/T_x$ for crystallization of the glass is shown in Fig. 14. The linear plot validates the kinetic model of

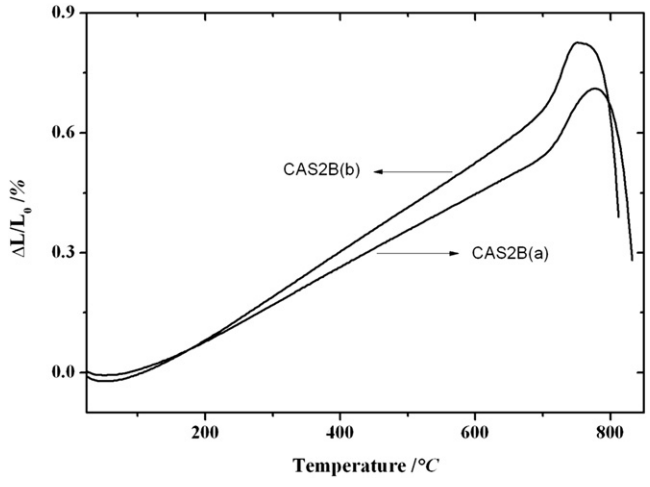

Fig. 13. TEC of CAS2B: (a) Before heat treatment $\alpha = 8.9 \times 10^{-6}$; (b) After heat treatment $\alpha = 11 \times 10^{-6}$.

Table 3
Effect of heating rate on DTA crystallization peak temperature (T_x) for CAS2BT glass.

Heating rate θ(°C min^{-1})	T_x (°C)	T_x (K)	$1/T_x$ ($\times 10^5$)	$\ln(T_X^2/\theta)$
1	980	1253.15	7.98	14.27
3	1021	1294.15	7.73	13.23
5	1031	1304.15	7.67	12.74
7	1049	1322.15	7.56	12.43
10	1068	1301.15	7.68	12.04
15	1076	1349.15	7.41	11.71
20 and 30	–	–	–	–

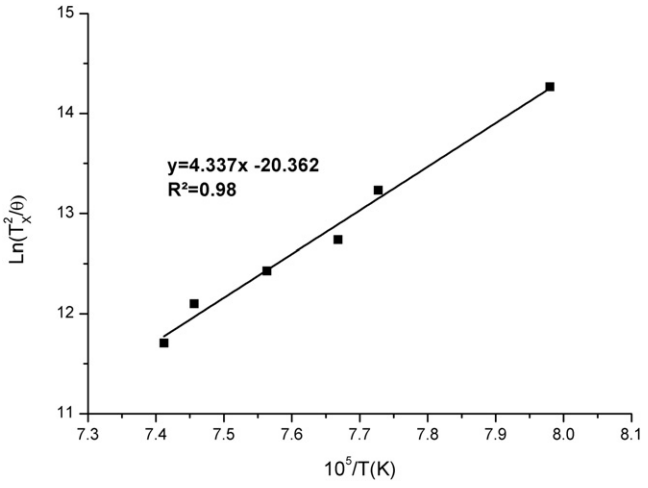

Fig. 14. $\mathrm{Ln}\left(\frac{T_x^2}{\theta}\right)$ versus $1/T_x$ for CAS2B glass $\Rightarrow E$ = Slope. R. 10^5.

Bansal et al. [30,32] and the assumptions made in this model. Values of kinetic parameters E and υ obtained from linear least squares fitting of the experimental data are listed in Table 4.

The Avrami parameter n can be evaluated from the non-isothermal data using the derived expression described by Piloyan et al. [33] (eq. (6)), which is valid in the range $0 < x < 0.2$:

$$\frac{\mathrm{d}\ln(\Delta y)}{\mathrm{d}(1/T)} = \frac{-nE}{\mathrm{R}} \tag{6}$$

and thus (eq. (7)):

$$\ln(\Delta y) = \frac{-nE}{\mathrm{R}}\left(\frac{1}{T}\right) + \mathrm{C} \tag{7}$$

Δy is the vertical displacement of the DTA crystallization exotherm from its baseline at different temperatures $T_C < T < T_x$, as shown in Fig. 15. T_C corresponds to the beginning of the peak. C is the constant of integration and n the Avrami parameter which gives an indication of the crystal growth mechanism in the glass.

The Piloyan plot of $\ln(\Delta y)$ versus $1/T$ for crystallization of CAS2B glass (Fig. 16) is linear. Deviations were observed at higher temperatures, as the Piloyan equation is valid only in the range $0 < x < 0.2$ (x is the volume fraction of the crystallized glass). The value of n obtained from least squares fitting of the linear portion of the data was 1.46. The value of n depends on the mechanism of the transformation reaction. Possible values of n for various mechanisms based on zero or constant nucleation rate are given in [32,33]. The n value of 1.45 in the present study corresponds to the one-dimensional growth of the first formed crystalline phase. Based on the morphologies of the phases which crystallize in the CAS2 system (Fig. 6a), it can be observed that only the $CaSiO_3$ phase shows one-dimensional growth of needle-shaped crystals. This indicates that $CaSiO_3$ is the first formed crystalline phase in CAS2B glass.

The crystallization activation energy of 360 kJ mol^{-1} obtained for CAS2B glass is much lower than 473–560 kJ mol^{-1} reported earlier for barium aluminosilicate (BAS) and strontium aluminosilicate (SAS) glass [34,35] as well as 420 kJ mol^{-1} for magnesium aluminoborosilicate (MABS) glass [36]. This major difference in activation energy is certainly due to the difference of the first crystalline phases formed in these various glass. The $CaSiO_3$ crystalline phase is formed first in CAS2BT glass whereas $BaAl_2Si_2O_8$ forms first in BAS, $SrAl_2Si_2O_8$ in SAS and $MgSiO_3$ in MABS glass. The activation energy of 360 kJ mol^{-1} in the present study is probably for the growth of $CaSiO_3$ crystals.

Table 4
Crystallization kinetic parameters for CAS2B glass using DTA.

Parameter	Value
Activation energy, E (kJ mol^{-1})	360
Frequency factor, ν (s^{-1})	1.33×10^{14}
Avrami parameter (n)	1.46

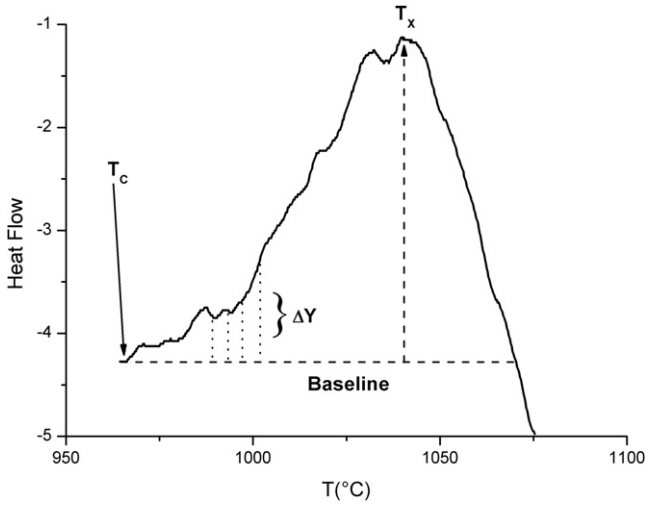

Fig. 15. Determination of the Δy displacement from the baseline on DTA crystallization peak.

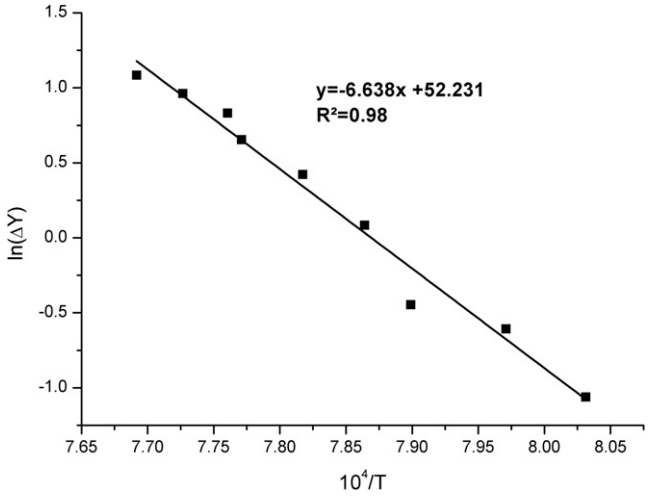

Fig. 16. $\ln(\Delta y)$ versus $1/T \Rightarrow n$ = (Slope. R. 10^5)/E.

4. Conclusions

Two glass compositions (CAS1 and CAS2) in the $CaO–Al_2O_3–SiO_2$ system with 6 wt% B_2O_3 were investigated to develop a glass ceramic for sealing SOECs. A comparative study based on physiochemical and thermal characterizations showed that the CAS2B glass composition meets most of the requirements for efficient sealing. CAS2B optimization tests by adding V_2O_5, K_2O and TiO_2 showed that V_2O_5 improves glass behavior at high temperature by reducing the viscosity while enhancing crystallization. Adding K_2O delays crystallization but increases the glass viscosity. TiO_2 addition has no significant effect on glass behavior. We concluded that the CAS2B composition is the most suitable for such applications. The choice of an optimal heat treatment is a compromise between delaying

crystallization induced by increasing the heating rate, and delaying the viscosity drop induced by decreasing the heating rate.

Dilatometry investigations shows that the TEC value measured for CAS2B glass ceramic is between that of Crofer® and YSZ, which is ideal to ensure solid sealing between these two materials.

Crystallization kinetic investigations identified and characterized the phases that crystallize in the CAS2B glass composition. The activation energy of glass crystallization was calculated to be 259 kJ mol^{-1}. Determination of the kinetic parameters showed that needle-shaped $BaSiO_3$ crystals are formed first, followed by other phases after longer heat treatment.

Acknowledgments

The authors are grateful to Charlène Vallat and Bruno Penelon from the CEA Marcoule DTCD/SECM/LDMC laboratory for the SEM observations, DTA and viscosity measurements, and to Emmanuelle Brackz of the CEA Marcoule DTEC/SGCS/LMAC laboratory for the microprobe results.

References

[1] S. Fujiwara, S. Kasai, H. Yamauchi, K. Yamada, S. Makino, K. Matsunaga, M. Yoshino, T. Kameda, T. Ogawa, S. Momma, E. Hoashi, Progress in Nuclear Energy 50 (2008) 422–426.
[2] T. Iwata, Y. Enami, Journal of the Electrochemical Society 145 (1998) 931–935.
[3] R.N. Basu, Recent Trends in Fuel Cell Science and Technology (2006) 284–329.
[4] J.W. Fergus, Journal of Power Sources 147 (2005) 46–57.
[5] C. Lara, M.J. Pascual, A. Durán, Boletin de la Sociedad Española de Cerámica y Vidrio 42 (2003) 133–144.
[6] K. Eichler, G. Solow, P. Otschik, W. Schaffrath, Journal of the European Ceramic Society 19 (1999) 1101–1104.
[7] K.S. Weil, Journal of Organometallic Chemistry 58 (2006) 37–44.
[8] P.A. Lessing, Journal of Materials Science 42 (2007) 3465–3476.
[9] S.S. Parihar, R.N. Singh, in: F. Dogan, P.N. Kumta (Eds.), Ceramic Transactions, Baltimore, MD (2006), pp. 157–164.
[10] Z. Dai, J. Pu, D. Yan, B. Chi, L. Jian, International Journal of Hydrogen Energy 36 (2011) 3131–3137.
[11] S. Sang, J. Pu, S. Jiang, L. Jian, Journal of Power Sources 182 (2008) 141–144.
[12] S. Sang, W. Li, J. Pu, L. Jian, Journal of Power Sources 177 (2008) 77–82.
[13] E.V. Stephens, J.S. Vetrano, B.J. Koeppel, Y. Chou, X. Sun, M.A. Khaleel, Journal of Power Sources 193 (2009) 625–631.
[14] L. Peng, Q. Zhu, Journal of Power Sources 194 (2009) 880–885.
[15] F. Smeacetto, M. Salvo, M. Ferraris, J. Cho, A.R. Boccaccini, Journal of the European Ceramic Society 28 (2008) 61–68.
[16] H.D. Ackler, Journal of the American Ceramic Society 81 (1998) 3093–3103.
[17] P. Hrma, W.T. Han, A.R. Cooper, Journal of Non-Crystalline Solids 102 (1988) 88–94.
[18] R.N. Singh, International Journal of Applied Ceramic Technology 4 (2007) 134–144.
[19] D. Coillot, F.O. Méar, R. Podor, L. Montagne, Advanced Functional Materials 20 (2010) 4371–4374.
[20] D. Coillot, R. Podor, F.O. Méar, L. Montagne, Journal of Electron Microscopy 59 (2010) 359–366.
[21] H. Khedim, A. Connelly, H. Nonnet, D. Coillot, F. Mear, L. Montagne, in: A.I.S.A. Technology, 12th International Ceramic Congress, Trans Tech Publication, Montecatini Terme, 2010, pp. 76–82.
[22] H. Nonnet, A. Connelly, H. Khedim, in: C.a.l.E.A.e.a.E. Alternatives (2010) France.
[23] M.J. Pascual, A. Durán, M.O. Prado, Physics and Chemistry of Glasses 46 (2005) 512–520.
[24] H. Scholze, Berichte der Deutschen Keramischen Gesellschaft 391 (1962) 63–68.
[25] H. Khedim, S. Abdelouhab, R. Podor, C. Rapin, M. Vilasi, in: Materials Science Forum, Les Embiez (2008), pp. 621–627.
[26] H. Khedim, R. Podor, C. Rapin, M. Vilasi, Journal of the American Ceramic Society 91 (2008) 3571–3579.
[27] N.P. Bansal, E.A. Gamble, Journal of Power Sources 147 (2005) 107–115.
[28] M. Avrami, The Journal of Chemical Physics 7 (1939) 1103–1112.
[29] H.J. Brochard, Journal of Inorganic and Nuclear Chemistry 12 (1960).
[30] N.P. Bansal, R.H. Doremus, A.J. Bruce, C.T. Moynihan, Journal of the American Ceramic Society 66 (1983) 233–238.
[31] N.P. Bansal, A.J. Bruce, R.H. Doremus, C.T. Moynihan, Journal of Non-Crystalline Solids 70 (1985) 379–396.
[32] N.P. Bansal, R.H. Doremus, Journal of Materials Science 20 (1985) 2794–2800.
[33] G.O. Piloyan, I.D. Ryabchikov, O.S. Novikova, Nature 212 (1966) 1229.
[34] N.P. Bansal, M.J. Hyatt, Journal of Materials Research 4 (1989) 1257–1265.
[35] M.J. Hyatt, N.P. Bansal, Journal of Materials Science 31 (1996) 172–184.
[36] D. Bahadur, N. Lahl, K. Singh, L. Singheiser, K. Hilpert, Journal of the Electrochemical Society 151 (2004).